Journal of Materials Chemistry A

Accepted Manuscript

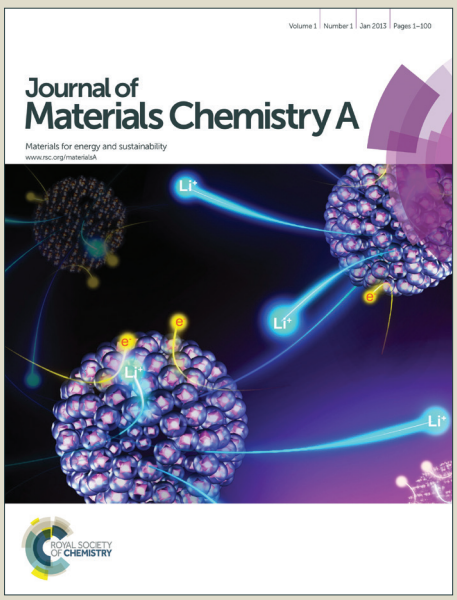

ROYAL SOCIETY OF CHEMISTRY

www.rsc.org/materialsA

Journal Name

ARTICLE

Oxygen deficient, carbon coated self-organized TiO_2 nanotubes as anode material for Li-ion intercalation

Received 00th January 20xx,
Accepted 00th January 20xx

DOI: 10.1039/x0xx00000x

www.rsc.org/

J. Brumbarov,[a] J. P. Vivek,[b] S. Leonardi,[a] C. Valero-Vidal,[c] E. Portenkirchner,[c,]* and J. Kunze-Liebhäuser[c]

Since several years, research for high capacity anode materials in Li-ion batteries is addressed to titanium dioxide (TiO_2), which offers important advantages in terms of cost effectiveness, safety and environmental compatibility. This work reports on the lithiation and delithiation characteristics of anodically grown, self-organized TiO_2 nanotubes annealed in Ar (TiO_{2-x}) and Ar/C_2H_2 (TiO_{2-x}-C). The systems are used as model composite electrodes for the anode in Li-ion batteries. Anatase TiO_{2-x}-C nanotubes demonstrate a superior Li storage capacity as high as 320(±68) mAh g^{-1} ($Li_{0.96}TiO_2$) compared to 180(±38) mAh g^{-1} ($Li_{0.54}TiO_2$) for TiO_{2-x}. This is comparable to the highest reported capacities for TiO_2 nanotubes to date. The double layer capacities are estimated from cyclic voltammetry measurements to 85 µF cm^{-2} for TiO_{2-x} and 20 µF cm^{-2} for TiO_{2-x}-C nanotubes respectively. Additionally, electrochemical impedance spectroscopy reveal smaller charge transfer resistances for TiO_{2-x}-C nanotubes at the solid/liquid interface which improves the transfer of Li^+-ions from the electrolyte into the electrode.

Introduction

Lithium ion batteries (LiBs) have been used in a wide variety of portable electric devices due to their high energy densities. However, they still need to be improved before they can be used in large-scale and high power applications. To improve kinetics, new nanostructured electrode morphologies, such as nanoparticles, nanofibers, nanowires and nanotubes (NT) having at least one nanometric dimension, have been considered.[1–3] Since several years, research for anode materials is addressed to titanium dioxide (TiO_2), which offers important advantages in terms of cost effectiveness, safety and environmental compatibility.[3,4] The lithium insertion potential of TiO_2 is between 1.2 V and 2.0 V vs. Li and lies within the stability window of common organic electrolytes, which leads to superior safety. TiO_2 shows a very low volume change (<1%) during cycling, which leads to high cycling stability, high rate, low-temperature charge/discharge capability and high thermal stability in both the charged and discharged state.[5] The lithiation reaction can be described by Equation 1:

$$TiO_2 + x\,(Li^+ + e^-) \rightleftharpoons Li_xTiO_2 \qquad (1)$$

The theoretical capacity of TiO_2 with anatase or rutile structure is 335 mAh g^{-1}, which corresponds to 1 mole (M) inserted lithium per mole TiO_2.[6] Reported capacity values correspond to x<1. For anatase and rutile powder, the theoretical value for a rate of 1C corresponds to 168 mA g^{-1},[7,8] which is 0.5 mole Li per mole TiO_2. Full lithiation can, up to now, only be achieved with particles smaller than 10 nm in diameter,[9,10] which is most likely due to a difference in diffusion coefficients in the dilute and fully lithiated forms of TiO_2.[11,12] Anatase has a tetragonal unit cell that can theoretically accommodate one lithium for every titanium. Upon lithiation to $Li_{0.5}TiO_2$, anatase is observed to undergo a tetragonal to orthorhombic phase transition. This composition is also most frequently reported as the maximum electrochemical insertion limit of Li into bulk anatase, although concentrations as high as 0.6 have been reported.[13–15] Only with nanostructured anatase TiO_2 has the theoretical capacity of x = 1.0 been reached.[10,16–18] The electrochemical performance of TiO_2 strongly depends on its morphology and its crystallographic structure. Due to the good intercalation characteristics of nanostructured TiO_2, the research on this material is focused on nanosized or nanotextured forms.[19–27] Nano-sized anatase TiO_2 has been in the focus of the majority of studies on Li insertion. Most of the work reporting high reversible intercalation capacities and high rate capabilities is based on the study of TiO_2 NT produced via the hydrothermal method. Some examples of the best performing hydrothermal nanotubular systems are listed hereafter: Xu et al.[28] observed a maximum reversible capacity of 238 mAh g^{-1} ($Li_{0.71}TiO_2$) in the first cycle, decaying to 198 mAh g^{-1} ($Li_{0.59}TiO_2$) in the 20th cycle. At high current

[a] Technische Universität München, Physik Department E19, James-Franck-Str.1, Garching, 85748, Germany.
[b] University of Liverpool, Stephenson Institute for Renewable Energy, Peach Street, Liverpool, L69 7ZF, United Kingdom.
[c] Leopold-Franzens-University Innsbruck, Institute of Physical Chemistry, Innrain 52c, Innsbruck, 6020, Austria.
† Electronic Supplementary Information (ESI) available: See
DOI: 10.1039/x0xx00000x

densities, the reported reversible capacities were lowered to 171 mAh g^{-1} ($Li_{0.51}TiO_2$) at 140 mA g^{-1} and to 168 mAh g^{-1} ($Li_{0.5}TiO_2$) at 210 mA g^{-1}. Higher reversible capacities of 248 mAh g^{-1} ($Li_{0.74}TiO_2$) in the first cycle and stable cycling performance at faster charge/discharge rates were reported by Li et al.[29] Additionally 293 mAh g^{-1} at 1C were reported for bronze poly-morph nano structures of titanium dioxide (TiO_2 - B) from Zhang. et. al.[16] and exceptionally high 415 mAh g^{-1} for TiO_2-B nanoparticles/double-walled NT (NP/DWNT) from Yang et. al.[18]

TiO_2 can be nanostructured by simple anodic oxidation in fluoride containing electrolytes to form highly ordered, self-organized TiO_2 NT,[30] a process that has been intensely studied and mostly understood in terms of its mechanism.[31,32] This electrochemical growth can lead to layers of parallel tubes with diameters of 30 to 200 nm and with a variable length of 0.3 to ~ 260 µm.[33] Self-organized and well oriented nanotube arrays are promising electrodes for Li-ion battery applications due to their oriented pore structure which is expected to facilitate one-dimensional electronic and ionic conduction and to accommodate volume changes during charge/ discharge cycling. The thin walls offer short solid-state Li-ion diffusion pathways and high tolerance to structural changes occurring during charge/ discharge cycling. For self-organized TiO_2 NT with sufficiently high electronic conductivity, no conductive binder is needed for the integration of the nanostructured electrodes in the cell because the NT are grown on Ti metal which itself serves as the current collector. This makes the system less complex and thus better suited for fundamental research than complex powder based electrodes and will most likely lead to a reduced electrode mass since all material is active as Li intercalation host. Despite these potential advantages of electrodes consisting of self-organized TiO_2 nanotube arrays, only a few studies report on their Li insertion characteristics.[21,34–40] Fang et al. found high rate capabilities for amorphous anodic TiO_2 NT, they observed discharge capacities of ~170 mAh g^{-1} at 10 A g^{-1} and ~140 mAh g^{-1} at 30 A g^{-1}.[36] Ivanov et. al. report high discharge capacities of about 200 mAh g^{-1}.[34] Wu et al. observed stable capacities for self-organized anatase TiO_2 NT of up to 230 mAh g^{-1} at a rate of C/3,[37] whereas Zhu et al. found 190 to 50 mAh g^{-1} only when the cycling rate was increased from 0.2 to 7 C.[38]

The effect of thermal annealing at temperatures up to ~400 °C in reducing atmosphere has been investigated previously on TiO_2 nanopowders used as negative electrodes for Li insertion[41] to overcome the relatively slow chemical diffusion of Li in TiO_2 which still limits its rate capability. While TiO_2 is semiconducting in its anatase or rutile form, a high temperature annealing in acetylene leads to conversion of the respective TiO_2 phase into a carbon rich conducting titanium oxycarbide.[42] Capacities of 234 mAh g^{-1} are reported for pristine TiO_2 nanoparticles and of 350 mAh g^{-1} for Ar annealed TiO_2 nanoparticles at 0.2 C; these two materials showed negligible Li insertion capacities at 10 C. However, high rate capability of Li storage has been reported for the oxygen-deficient TiO_x (x<2) nanoparticles prepared by hydrogen reduction, which showed 70 - 130 mAh g^{-1} at 10 C, depending on the annealing conditions. This study on the effect of electronic charge carrier concentration on the overall electrochemical Li storage performance revealed that well-balanced Li^+/e^- transport is a key factor for high performance TiO_2 anodes. Additionally, the effect of hydrogen annealing has also been studied for the Li insertion in anodic TiO_2 NT:[40] an improvement of the rate capability was found and interpreted as a result of increased electronic conductivity of the nanotube bulk due to the formation of oxygen vacancies. In this study, the highest reported initial discharge capacity for reduced TiO_x NT at a slow insertion rate of 5 µA cm^{-2} (~4.7 mA g^{-1}, corresponding to about 0.015C) was 0.274 mAh cm^{-2} (~259 mAh g^{-1}), the coulombic efficiency was 87.1 %. At the highest rate investigated of 2000 µA cm^{-2} (~1880 mA g^{-1}), the capacity dropped to 0.072 mAh cm^{-2} (68 mAh g^{-1}). Liu et al. performed thermal annealing of TiO_2 NT at 400°C in CO and N_2 gas. They report an initial discharge capacity of 223 mAh g^{-1} at a rate of 320 mA g^{-1} for the CO annealed tubes which decreased to 179 mAh g^{-1} after 50 cycles [39]. In recent work on Li-intercalation in percolating networks of TiO_2 nanorods and carbon, storage capacities of 250 mAh g^{-1} have been observed during cycle tests at 1 C, which is explained by the nanosized dimensions of the rods where complete formation of $LiTiO_2$ can be achieved.[8]

In the present work, self-organized TiO_2 NT were grown electrochemically, annealed at 400°C in acetylene containing gas atmosphere to form oxygen vacancies and a thin carbon coating, and used as negative electrodes for Li insertion. The nanotube arrays are self-organized on a Ti metal sheet that is used as current collector and support, therefore no conductive carbon additive is necessary in our experiments. Thus no additional effects of nanoparticle packing and connectivity can occur that are normally found in studies where inks of active material, conductive carbon, a polymeric binder and a solvent are used.[5,41] Galvanostatic charge/ discharge experiments showed that the Li storage capacity of this system is remarkably high, reaching the theoretical capacity of $x \approx 1.0$ (forming $LiTiO_2$).

Experimental

Reagents, solutions and electrode materials

TiO_2 NT were grown electrochemically on mechanically polished (4000P SiC grinding paper) titanium (Ti) discs (99.6% Advent) by exposing the polished surface (50.3 (± 6.7) mm^2) to an electrolyte containing 50 vol. % ethylene glycol (99.5% EMSURE, Merk) in deionized (DI) water (18.2 MΩ cm Milli-Q, Millipore) and 2 wt. % NH_4F (99.99%, Merk) and applying an anodic potential of 20 V by scanning from 0 V with a ramp rate of 1 V s^{-1} for 1 h. After anodization, the sample was immediately removed from the electrochemical cell and thoroughly rinsed with DI water.

In order to increase the electronic conductivity and modify the Li intercalation properties of the as grown amorphous TiO_2 NT, carbo-thermal reduction was carried out in a horizontal tube furnace: the quarz reactor tube was first thoroughly purged

with Ar (4.8, Linde) at room temperature (RT) to remove air. The Ar flow was then reduced to 200 sccm and held constant until the end of the annealing procedure. 5 sccm acetylene (solvent-free, Linde) were added to the Ar flow for 3 min before increasing the temperature. To avoid thermal stress during temperature increase, the ramping speed was gradually reduced from 10°C min^{-1} up to 200°C, to 5°C min^{-1} up to 300°C and finally 3°C min^{-1} up to 400°C. After 20 min dwell time at 400°C, 0.1 sccm acetylene was added to the Ar flow for 1 h. The system was then held at 400°C for another 280 min to allow for complete transformation of the NT and then cooled down to RT with 3°C min^{-1}. For the production of TiO_{2-x} anatase nanotube references, the same annealing procedure was conducted in pure Ar without acetylene.

Measurements and Instrumentation

All electrochemical measurements were carried out in a three electrode T-cell with PFA body and sealing rings (Union Tee Tube Fitting PFA-820-3, Swagelok) and stainless steel current collectors (316 stainless steel) for contacting working (WE), counter (CE) and reference (RE) electrodes. Lithium foil (99.9%, Alfa Aesar) was used as CE and RE. The self-organized TiO_{2-x} and TiO_{2-x}-C nanotube arrays that were anodically grown on Ti metal sheets and annealed under Ar and Ar/C_2H_2 were directly mounted as WE in the electrochemical cell, without adding conductive carbon, placing the Ti sheet as current collector on the stainless steel rod. Working and counter electrode were separated by one layer of Celgard separator soaked with electrolyte. The electrolyte (SelectiLite battery electrolyte LP 30, Merck) used in all measurements was 1mole $LiPF_6$ in a 1:1 (w/w) mixture of ethylene carbonate (EC) and dimethyl carbonate (DMC) which is stable in the potential range 1.1 to 3.0 V vs. Li/Li^+ used in this study. All potentials herein are given with respect to the Li/Li^+ reference electrode unless stated otherwise. All cells were assembled in an Ar filled glove box with a water and oxygen content below 0.1 ppm. The assembled cells were connected to a potentiostat (BioLogic VSP) outside the glove box, and all measurements were performed at room temperature.

Cyclic Voltammetry (CV) measurements were performed with a scan rate of 0.1 mV s^{-1} between 1.1 and 3.0 V. Galvanostatic Cycling with Potential Limitation (GCPL) was carried out between 1.1 to 3.0 V at current densities of 50, 100, 200, 500 and 1000 mA g^{-1} corresponding to lithiation/ delithiation rates of 0.3, 0.6, 1.2, 3 and 6 C, respectively. The mass of the active material anatase TiO_2 is estimated by measuring the volume of the NT solid fraction and by using the TiO_2 anatase density of 3.84 g cm^{-3} (for simplicity the value of 3.9 g cm^{-3} was used for the calculations) to calculate the mass of the solid fraction. The current dependent gravimetric specific capacity for lithiation/ delithiation and the corresponding columbic efficiency (delithiation capacity over lithiation capacity) was determined from these measurements. Electrochemical impedance spectroscopy (EIS) was performed at open circuit potential (OCP) before CV and GCPL and ranged from 100 kHz to 0.5 Hz with a peak-to-peak amplitude of ±5 mV. Ohmic and electron transfer resistances together with their corresponding capacitive elements, can be extracted from the impedance data, which allows to control possible interface changes of the electrode. Error estimations regarding the calculation of active electrode volume and mass were done by applying the Gaussian error propagation with independent parameters. Additionally, the geometric uncertainty in the active electrode diameter was estimated by 8 (± 0.5) mm.

Morphological changes of the electrodes were monitored by comparing scanning electron microscopy (SEM) (CrossBeam NVision 40, Zeiss) micrographs before and after nanotube conversion through annealing and Li insertion/ extraction. SEM micrographs were taken with a Zeiss SUPRA™ 40 field emission SEM based on the 3rd generation GEMINI® column. To determine the chemical composition of the surface after the thermal treatments in pure Ar and in the Ar/C_2H_2 mixture, X-ray photoelectron spectroscopy (XPS) measurements were carried out with a Specs Phoibos 100 hemispherical electron energy analyzer and a MCD-5 detector. The take-off angle was 0 relative to the surface normal and an Al Kα X-ray source (1486.6 eV) without monochromator was used. High resolution spectra were recorded for the Ti 2p, C 1s and O 1s regions with a step size of 0.025 eV and a dwell time of 0.5 s. Quantitative analysis was performed using CasaXPS software (version 2.3.14dev38).[43] Structural and compositional information about the reduced titania films was obtained by grazing incidence diffraction (GID). The GID analysis was performed on a Bruker D8 Advance Diffractometer, equipped with a Soller Slit on the detector. The optimal incidence angle was found to be 2. Diffractograms were acquired between 20 and 60 degree (2 theta) with a step size of 0.02 and an acquisition time of 60 s per step.

Results and Discussion

Nanotube morphology, structure and chemical composition

Figure 1 depicts scanning electron micrographs of the TiO_2 NT before and after annealing to TiO_{2-x} in Ar and to TiO_{2-x}-C in an Ar/C_2H_2 mixture. From the SEM micrographs, 1 µm average tube length, 18 nm average wall thickness and 120 nm average pore diameter, and a solid hemisphere at the bottom of each tube are determined. X-ray diffraction (XRD) measurements (compare Figure S1 in the supporting information) reveal TiO_2 anatase structure of the NT after their conversion in Ar and in Ar/C_2H_2 at 400°C. A crystallite size of ~30 nm of anatase TiO_2 has been calculated from the broadening of the diffraction line of the (101) plane at 25.2° using the Scherrer equation, which is in accordance with former findings.[38,44,45] In case of TiO_x, small changes in crystallinity have been observed after Li insertion: the anatase (A) (200) signal disappears, and the A (101) signal decreases in intensity. On TiO_{2-x}-C, no remarkable differences are observed after lithiation. There is no visible change in morphology after both annealing processes, therefore we assume that the carbon layer induced by annealing in Ar/C_2H_2 mixtures is very thin and forms at the outside of the NT only.

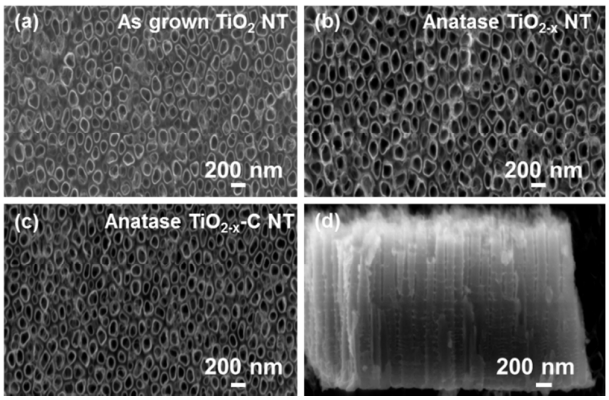

Figure 1. SEM images of TiO_2 NT before and after annealing. (a) as grown TiO_2 NT, (b) after annealing to TiO_{2-x} in Ar, (c) after annealing to TiO_{2-x} -C in an Ar/C_2H_2 mixture and (d) cross-section of TiO_{2-x} –C.

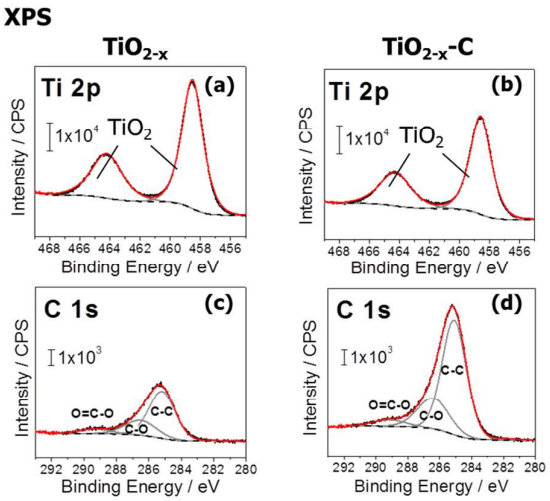

Figure 2. High resolution XPS spectra of TiO_{2-x} and TiO_{2-x}-C NT. (a,c) Ti 2p and C 1s signals of TiO_{2-x}, (b,d) Ti 2p and C 1s signals of TiO_{2-x}-C.

X-ray induced photoelectron spectroscopy (XPS) measurements support these findings (see **Figure 2**). The Ti 2p peak shows the presence of TiO_2 at the surface, TiC or sub-oxides are not detected. The NT annealed in Ar/C_2H_2 show an increased amount of carbon at the surface with a TiO_2:C ratio of 93:7 at % for TiO_{2-x} and 82:12 at % for TiO_{2-x}-C (Figure 2).

The mass of the active material anatase TiO_2 is estimated by measuring the volume of the NT solid fraction and by using the TiO_2 anatase density to calculate the mass of the solid fraction. The dimensions and the number of NT per unit area are determined from the SEM images. For determining the active electrode mass, including a geometric electrode diameter uncertainty of ± 0.5 mm and the standard deviation in tube volume by 0.89 x 10^6 nm^3, 10% additional mass is assumed to get the final number of 138 (±37) µg, used for the calculations. This method is comparable to that used in other studies of Li insertion in anodic TiO_2 NT.[37,38] For comparability of our data with data given as areal capacities, we report both values in **Table 1**.

Electrochemical Impedance Spectroscopy and Cyclovoltam-metry

Prior to electrochemical experiments, electrochemical impedance spectroscopy (EIS) data were recorded at the open circuit potential (OCP) inside the electrolyte that was used for the lithiation measurements (**Figure 3**). Steady-state conditions were assured during EIS measurements since the OCP value of 2.61 V vs. Li/Li^+ is maintained practically constant. From the Nyquist plots, electronic elements (the ohmic and electron transfer resistances together with capacitive elements) of the studied system were determined by fitting the experimental spectra to the equivalent circuit shown in Figure 3 (b). Constant phase angle elements (CPE) are introduced to replace real capacitors and to account for the non-ideal behavior of all capacitive elements.[46,47] In the equivalent circuit, R_s is the ohmic solution resistance arising from the movement of Li^+ ions in the electrolyte solution.

R_{ct} is the surface charge transfer resistance and CPE_{dl} is related to the double layer capacitance, which are processes taking place at the interface between the TiO_2 NT and the electrolyte. R_{Li} is the lithiation-reaction resistance occurring upon Li^+ ion diffusion through the solid electrode material, and CPE_{Li} corresponds to the capacitive contribution of inserted Li^+ ions before the lithiation reaction is accomplished. CPE_{μ} is associated with the chemical capacitance of TiO_2 reacting with the Li^+ ions. A more detailed description of these elements used in the equivalent circuit can be found in [48,49]. The proposed equivalent circuit demonstrates excellent fitting congruency in the Nyquist and Bode plots (Figure 3a. and Figure S2 in the supporting information), with a mean square deviation (X^2) of 2.8 x 10^{-3} for TiO_{2-x} and 0.01 for TiO_{2-x}-C NT. A detailed summary of all fitting parameters is given in Table S1 in the supporting information.

Ohmic resistances of 3.2 Ω and 2.1 Ω are measured for TiO_{2-x} and TiO_{2-x}-C NT, respectively. Both resistive elements are extracted at the highest frequency domain where the impedance is independent of the frequency. These results suggest low solution resistance of the species through the electrolyte as well as good cell assembly. At higher frequency, a flat semicircle is detected in both spectra related to the interfacial charge transfer resistance (R_{ct}) in parallel combination with the double layer capacitance (C_{dl}). The surface charge transfer resistances (R_{ct}) of the Li^+ intake from the electrolyte into the nanotube bulk material are 104 Ω for TiO_{2-x} and 54 Ω for TiO_{2-x}-C. Due to the smaller charge transfer resistances of TiO_{2-x}-C NT at the solid/liquid interface, the transfer of Li^+-ions from the electrolyte into the electrode should be improved. The low electron transfer resistance of anatase TiO_{2-x}-C NT is most-likely attributed to the thin carbon film at the outside of the nanotube walls, additionally oxygen vacancies in the material enable fast ion and electron transfer.

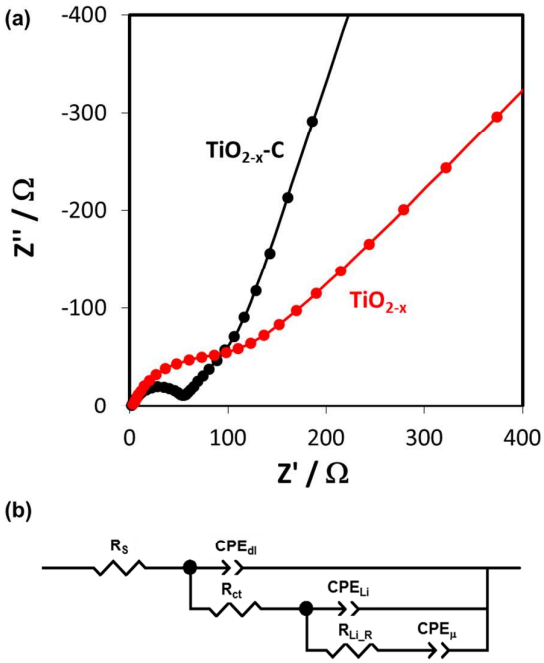

Figure 3. (a) Nyquist plots from EIS data for TiO2-x and TiO2-x-C NT together with their corresponding fitting curves. EIS was performed at open circuit potential (OCP) from 100 kHz to 0.5 Hz with a peak-to-peak amplitude of ±5 mV. (b) Corresponding equivalent electrical circuit.

At low frequencies, the TiO_{2-x} nanotube impedance shows a Warburg behavior (confirmed by *n* factor close to 0.5) indicating diffusion limitation of Li insertion/extraction into the bulk material. The Warburg prefactor for TiO_{2-x} is determined with 824, while for TiO_{2-x}-C it is 215 (compare Figure S3 in the supporting information), indicating that the effective chemical diffusion coefficient of Li increases upon C_2H_2 annealing.[41] In addition, the increase of the C_μ in TiO_{2-x}-C NT indicates that an enhancement of the Li^+-ion storage inside the material could be favored.

The time constant at intermediate frequency appears more defined in the Nyquist plot of TiO_{2-x}-C NT, which suggests that different intercalation reaction processes take place in the TiO_{2-x} and TiO_{2-x}-C NT. This is reflected in the increase of the capacitive element C_{Li} in the TiO_{2-x}-C NT (values shown in Table S1), thus indicating different contribution of inserted Li^+ ions moving inside the TiO_2 matrix before reaching stable sites. Once stable sites are reached the final lithiation reaction is accomplished to form Li_xTiO_2, as previously described in ref. nr. [48].

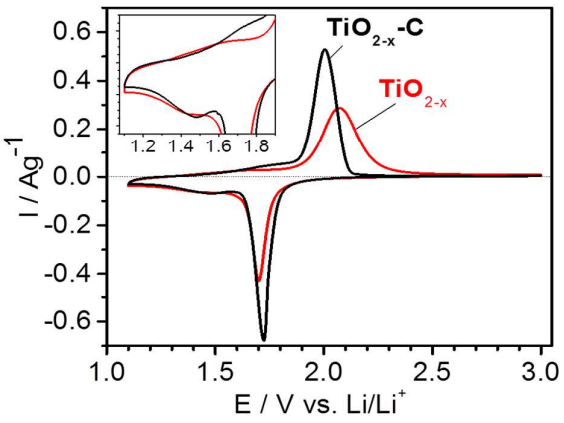

Figure 4. CVs (first cycles) of anatase TiO_{2-x}-C and TiO_{2-x} NT between 3.0 and 1.1 V, with a scan rate of 0.1 mV s^{-1}, showing lithiation/delithiation peaks at 1.70/ 2.07 V (TiO_{2-x}) and at 1.72/ 2.00 V (TiO_{2-x}-C). Inset: Second, small peak pair at 1.48 and ~1.75 V (shoulder) for both materials.

Figure 4 shows a CVs (first cycles) of anatase TiO_{2-x}-C and TiO_{2-x} NT. The materials show peak couples at 1.70/ 2.07 V (TiO_{2-x}) and at 1.72/ 2.00 V (TiO_{2-x}-C), that represent lithiation and delithiation, and that are in good agreement with peak positions reported in literature.[8,15,21,50] The main peak pair corresponds to lithiation and delithiation in the TiO_2 host structure.[15,50] The Li insertion into anatase TiO_2 is a two phase process, in which two phases, being Li-poor $Li_{0.01}TiO_2$ and Li-rich $Li_{0.55}TiO_2$ coexist. The hysteresis between lithiation and delithiation peak is smaller in the case of TiO_{2-x}-C NT, which is most likely due to their smaller charge transfer resistance at the solid/liquid interface. In addition to the main peaks, a second small peak pair is visible at 1.48 and ~1.75 V (shoulder) for both materials; this peak pair is more pronounced in case of TiO_{2-x}-C (inset in Figure 4). The second small peak pair is indicative for a second phase transition from $Li_{0.55}TiO_2$ to fully lithiated $LiTiO_2$, which can take place at RT in nanosized material with particle sizes <10 nm.[9,10]

Galvanostatic cycling

Galvanostatic cycling is carried out between 3.0 and 1.1 V (**Figure 5**). The reversible capacity of anatase TiO_{2-x} in the third cycle (Figure 5a) at the low rate of 0.3C (50 mA g^{-1}) is 180(±38) mAh g^{-1} ($Li_{0.54}TiO_2$), that of anatase TiO_{2-x}-C is as high as 320(±68) mAh g^{-1} ($Li_{0.96}TiO_2$). Irreversible capacities of 13(±2.8) and 21(±4.5) mAh g^{-1} are measured in cycle three, which are due to Li trapping inside the material.[51]

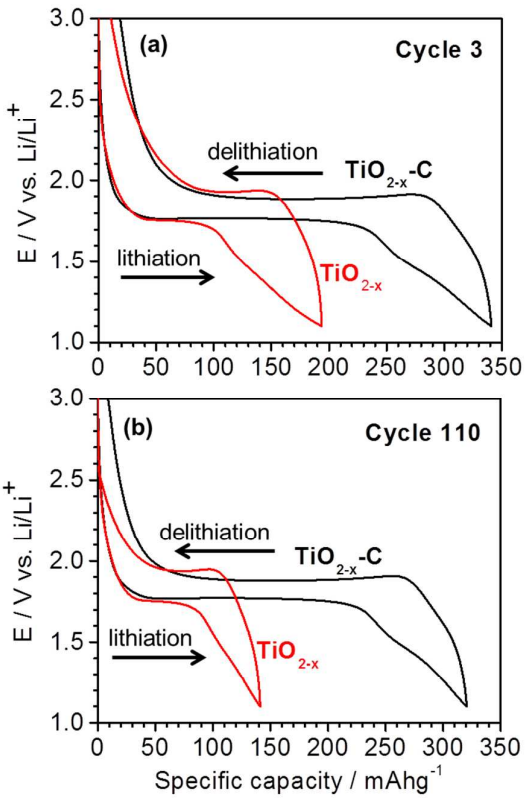

Figure 5. Galvanostatic charge/discharge curves of TiO_{2-x}-C and TiO_{2-x} NT (a) third cycle and (b) 110th cycle, between 3.0 and 1.1 V.

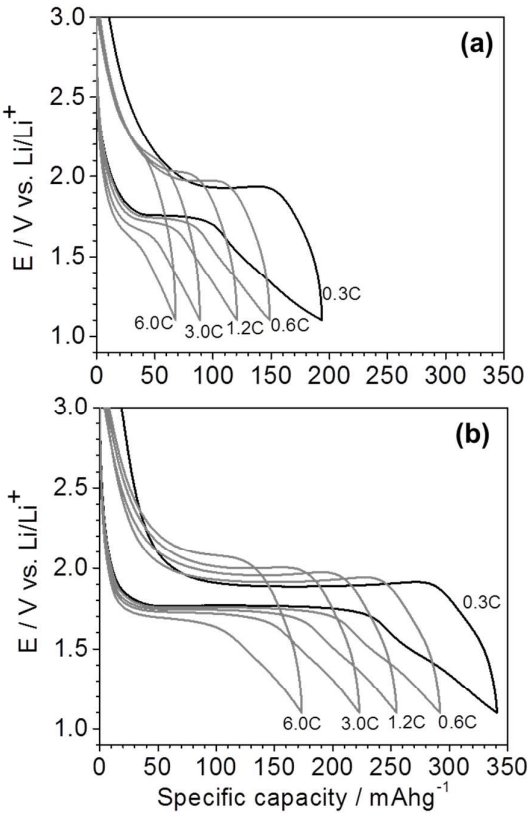

Figure 6. Galvanostatic charge-discharge curves (third cycles) of (a) TiO_{2-x} and (b) TiO_{2-x}-C NT recorded with different C-rates of 50 mA g^{-1} (0.3 C), 100 mA g^{-1} (0.6 C), 200 mA g^{-1} (1.2 C), 500 mA g^{-1} (3 C), 1000 mA g^{-1} (6 C);

The irreversible capacity loss is typically attributed to the trapping of Li^+ at defect sites of anatase TiO_2 nanostructures and/or the irreversible reaction of Li^+ with adsorbed water molecules.[28,52–54] In cycle 110 (Figure 5b), reversible capacities of 141(±30) and of 313(±66) mAh g^{-1} and irreversible capacities of 0 and 11(±2.3) mAh g^{-1} are measured for TiO_{2-x} and TiO_{2-x}-C. The double layer capacities are estimated from CV measurements to 85 µF cm^{-2} for TiO_{2-x} and 20 µF cm^{-2} for TiO_{2-x}-C NT, respectively. These values are in the range of typical double layer capacitances reported in literature[3,55] and hence verify the correct determination of the active electrode mass from SEM images (Figure 1).

Figure 6 depicts charge-discharge curves measured at different C-rates. For TiO_{2-x}, capacities of 146(±31) ($Li_{0.44}TiO_2$ at 0.6 C), 118(±25) ($Li_{0.35}TiO_2$ at 1.2 C), 84(±18) ($Li_{0.25}TiO_2$ at 3 C), and 64(±14) mAh g^{-1} ($Li_{0.19}TiO_2$) at 6 C are determined. For TiO_{2-x}-C, capacities as high as 285(±61) ($Li_{0.85}TiO_2$ at 0.6 C), 249(±53) ($Li_{0.74}TiO_2$ at 1.2 C), 214(±46) ($Li_{0.64}TiO_2$ at 3 C), and 162(±35) mAh g^{-1} ($Li_{0.48}TiO_2$ at 6 C) are observed, which demonstrates a very high rate capability of the material.

The discharge, which corresponds to the Li^+ insertion process, of TiO_{2-x}-C NT at 0.3 C can be described by three different regions: (1) a steady voltage decrease between 3.0 V and 1.77 V, which corresponds to a capacity of ~50 mAh g^{-1}, (2) a long plateau of ~152 mAh g^{-1} at 1.77 V; and (3) a voltage decrease from 1.8 V to 1.1 V, where additional 139 mAh g^{-1} of Li are inserted. The capacity observed for region (1) corresponds to ~0.15 mole Li per mole TiO_2, which agrees with the domain of the Li-poor solid solution phase already reported for TiO_2 nanoparticles, characterized by a very large fraction of insertion sites close to the materials surface.[9,56,57] Region (2) shows the plateau associated with the Li-poor to Li-rich phase transformation. Its capacity corresponds to the formation of $Li_{0.55}TiO_2$.[9,56] In region (3), the second phase transformation from Li-rich to $LiTiO_2$ takes place.[9,58] The transition to the fully lithiated phase is indicated by a small plateau at ~1.5 V (see Figure 6b).[57] At 0.3 C discharge rate the final composition achieved is $Li_{0.96}TiO_2$, which is close to the theoretical full lithiation. In case of TiO_{2-x}-C, the small plateau disappears at a discharge rate of 6 C, which means that $Li_{0.55}TiO_2$ is the phase with the highest achievable Li content, because the second phase change is kinetically limited; our data strongly support this assumption, because we observe the phase $Li_{0.66}TiO_2$ at 3 C and $Li_{0.51}TiO_2$ at 6 C. For TiO_{2-x}-C, the long plateau (region (2)) is still well defined for the highest rate

of 6 C. For TiO_{2-x}, the small plateau indicating full lithiation is less pronounced and cannot be observed at 1.2 C any more. The long plateau (region (2)) starts to disappear at 6 C. For both TiO_{2-x} and TiO_{2-x}-C nanotube arrays, the length of this plateau is comparable for lithiation and delithiation, which means that Li insertion and extraction have very similar kinetic limitations.

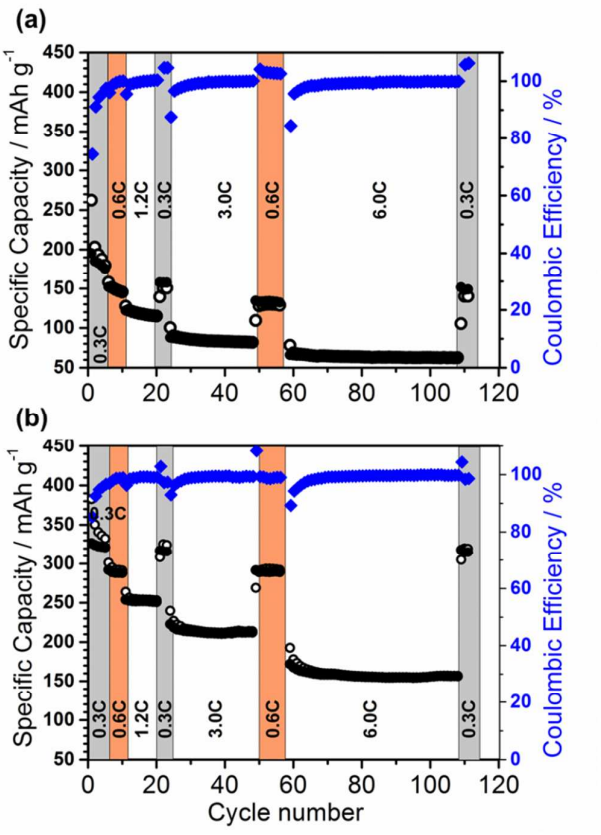

Figure 7. Gravimetric capacities (circles) and corresponding coulombic efficiencies (diamonds) of (a) TiO_{2-x} and (b) TiO_{2-x}-C NT as a function of cycle number for 110 cycles at different charge/discharge rates (0.3 C, 0.6 C, 1.2 C, 3 C, 6 C), between 3.0 and 1.1 V. Open circles: discharge (lithiation), closed circles: charge (delithiation).

Figure 7 shows the gravimetric capacities of (a) TiO_{2-x} and (b) TiO_{2-x}-C NT as a function of cycle number for 110 cycles at different charge/discharge rates between 3.0 and 1.1 V. The stable capacity at different rates shows that both systems have a very stable cyclability within the investigated potential range. For TiO_{2-x} NT, 81% and for TiO_{2-x}-C 97% capacity retention are obtained between cycle 2 and cycle 110 that are both recorded at 0.3 C. At 6 C (cycle number 100), the current efficiency is 99.93% for TiO_{2-x} NT at a capacity of 63(±13) mAh g^{-1} ($Li_{0.19}TiO_2$) and 99.98% for TiO_{2-x}-C NT at a capacity of 156(±33) mAh g^{-1} ($Li_{0.47}TiO_2$), which demonstrates the high rate capability of self-organized TiO_{2-x}-C NT. Table 1 summarizes the gravimetric and areal charge capacities measured for TiO_{2-x} and TiO_{2-x}-C NT at different C rates.

The reason for the much higher capacities and better rate-capability of TiO_{2-x}-C NT is assumed to be caused by the thin carbon film covering the outer wall of the tubes and by the oxygen vacancies produced in the TiO_2 bulk material upon carbo-thermal annealing. The carbon film most-likely enables fast electron transport via the surface film and does at the same time not hinder the Li^+ ions from entering the nanotube structure during Li intercalation.[21] To better understand the high Li storage capacities and high rate-capabilities presented in this study, we compared our findings with theoretical work in which thermodynamic and kinetic predictions are provided.[11] The authors report a very low diffusion coefficient calculated for the fully lithiated phase $LiTiO_2$ which explains the limited capacity of anatase electrodes in general. Their thermodynamic predictions indicate that $LiTiO_2$ forms through a two-phase reaction from $Li_{0.5}TiO_2$ to $Li_{0.58}TiO_2$. Mechanistically, this means that the fully lithiated phase forms at the surface of the electrode material and grows inward consuming the $Li_{0.58}TiO_2$. New Li for the reaction must diffuse through $LiTiO_2$, which covers the surface, to the phase boundary, which is suppressed due to the extremely low diffusion coefficient in this phase. This limits the maximum Li concentration of anatase, which is in agreement with experimental results.[14,15,59] Higher concentrations of Li are only possible for small nanoparticles of anatase, when diffusion distances are so small that diffusion is no longer rate-limiting.[22,60,61] The high Li concentrations measured in the present study are therefore possible due to the nano-sized wall dimensions (~10-20 nm) of the anodic TiO_2 NT. Moreover, the self-organized aligned NT seem to provide an ideal morphology for the two-phase reaction occurring to transform the Li-poor ($Li_{0.01}TiO_2$) to the Li-rich ($Li_{0.55}TiO_2$) phase. Crystallographic considerations showed that the Li-rich phase has two strain invariant planes that are parallel to the a-axis of the anatase unit cell, which is the direction of Li-diffusion in this phase. Therefore, Li diffusion in the Li-rich phase can only occur parallel to the reaction front and not toward the reaction front itself, hence the Li must be supplied from the Li-poor side of the reaction front. This is only possible if the Li-poor phase extends to the surface of the electrode throughout the two-phase reaction to allow new Li to enter the crystal.[11,12]

Table 1. Gravimetric and areal charge (delithiation) capacities measured for TiO_{2-x} and TiO_{2-x}-C NT at different C rates.

	0.3 C			
	Cycle 2		Cycle 110	
	mAh g^{-1}	mAh cm^{-2}	mAh g^{-1}	mAh cm^{-2}
TiO2-x NTs	185(±39)	0.05(±0.01)	148(±32)	0.04(±0.01)
TiO2-x-C NTs	324(±69)	0.08(±0.02)	313(±66)	0.08(±0.02)
	6 C			
	Cycle 100			
	mAh g^{-1}	mAh cm^{-2}		
TiO2-x NTs	185(±39)	0.05(±0.01)		
TiO2-x-C NTs	324(±69)	0.08(±0.02)		

Therefore, particles that show a core-shell growth behaviour where the Li-rich phase covers the whole particle are expected to suppress the Li supply to the moving interface. It is desirable that the moving interface extends to the surface of the particle to ensure completion of the two-phase reaction, so that Li-poor material is always exposed to the electrolyte to have Li entering the crystal. This is likely to occur in flat, plate-like particles that are thin in the [001] direction (parallel to the c-axis of the anatase unit cell).[11]

Self-organized anodic TiO_2 NT annealed to anatase have been analyzed in terms of their phase composition and orientation by Falaras et al. using polarized micro-Raman spectroscopy.[62] Even though the findings show a partial preferential orientation effect, i.e. not all but most of the crystallites of one nanotube show the same orientation, a general trend can be deduced, which showed that the self-organized NT growth direction is the [101] direction. Theoretical predictions by Belak et. al. [11,12] suggest that highest capacities should be observed if (001) planes are exposed to the electrolyte. This can be rationally understood since the moving interface between the Li-poor and Li-rich TiO_2 phase would always extend to the surface of the NT so that Li-poor TiO_2 is always exposed to the electrolyte, enabling new Li to enter the crystal.

In this context it is noteworthy that considerable fluctuations in the gravimetric capacities are measured over a large variety of samples tested, which can then be explained either by a mechanical detachment of the NT from the Ti-substrate upon lithiation and/or by the above mentioned preferential orientation of the NT ensuring an increased amount of (001) planes exposed to the electrolyte. Due to these considerations it is of critical importance to understand the influence of tube orientation on their lithiation capacities. This will be a main focus of ongoing studies in our laboratory.

Figure 8 depicts scanning electron micrographs of TiO_{2-x} and TiO_{2-x}-C NT after 100 Li lithiation/delithiation cycles. As can be seen, the tube morphology is not changed after Li insertion and extraction for both materials. The micrographs have a slightly blurry character, which is most likely caused by contaminants from the electrolyte solution that could not be completely removed after cycling.

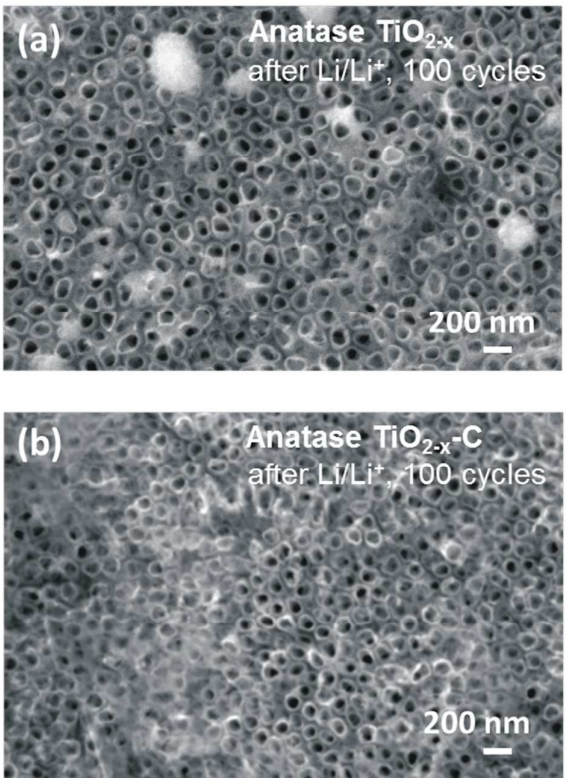

Figure 8. SEM micrographs of (a) TiO_{2-x} and (b) TiO_{2-x}-C NT after 100 lithiation/ delithiation cycles.

Conclusions

Lithiation and delithiation in anodically grown, self-organized TiO_2 NT annealed in Ar (TiO_{2-x}) and Ar/C_2H_2 (TiO_{2-x}-C) revealed that the TiO_{2-x}-C NT have a superior Li storage capacity as high as 320(±68) mAh g^{-1} ($Li_{0.96}TiO_2$) compared to 180(±38) mAh g^{-1} ($Li_{0.54}TiO_2$) for TiO_{2-x} NT. Additionally, TiO_{2-x}-C NT demonstrate a higher rate capability which makes them suitable for high energy and high power Li insertion electrodes. The double layer capacities are estimated from cyclic voltammetry measurements to 85 µF cm^{-2} for TiO_{2-x} and 20 µF cm^{-2} for TiO_{2-x}-C NT, respectively. Electrochemical impedance spectroscopy reveal smaller charge transfer resistances of TiO_{2-x}-C NT at the solid/liquid interface which improves the transfer of Li^+-ions from the electrolyte into the electrode.

Self-organized TiO_{2-x}-C NT are an important model-system as anode material for Li-ion batteries because they are directly grown electrochemically on a Ti sheet serving as current collector. These structures possess sufficiently high electronic conductivity, thus no conductive binder is needed for the integration of the nanostructured electrodes in the cell. The potential window of operation from 3.0 to 1.1 V is within the electrochemical stability range of commonly used electrolytes, which insures safe operation of the system. Furthermore, these nanostructured anode materials are among the best reported to date with respect to reversible capacity, long-term cyclability and rate performance.

Fluctuations in the measured gravimetric capacities of TiO_2 NT may be explained by a preferential orientation of the NT ensuring an increased amount of (001) planes exposed to the electrolyte. The effect of preferential orientation of TiO_2 NT on their lithiation capacities will therefore be a main focus of ongoing studies in our laboratory.

References

1 A. S. Aricò, P. Bruce, B. Scrosati, J.-M. Tarascon and W. van Schalkwijk, *Nat. Mater.*, 2005, **4**, 366–377.
2 P. G. Bruce, B. Scrosati and J.-M. Tarascon, *Angew. Chem. Int. Ed. Engl.*, 2008, **47**, 2930–2946.
3 K. Lee, A. Mazare and P. Schmuki, *Chem. Rev.*, 2014, **114**, 9385–454.
4 M. Kapilashrami, Y. Zhang, Y. Liu, A. Hagfeldt and J. Guo, *Chem. Rev.*, 2014, **114**, 9662–707.
5 B. Scrosati and J. Garche, *J. Power Sources*, 2010, **195**, 2419–2430.
6 S. Goriparti, E. Miele, F. De Angelis, E. Di Fabrizio, R. Proietti Zaccaria and C. Capiglia, *J. Power Sources*, 2014, **257**, 421–443.
7 M. Mancini, P. Kubiak, J. Geserick, R. Marassi, N. Hüsing and M. Wohlfahrt-Mehrens, *J. Power Sources*, 2009, **189**, 585–589.
8 D. Bresser, E. Paillard, E. Binetti, S. Krueger, M. Striccoli, M. Winter and S. Passerini, *J. Power Sources*, 2012, **206**, 301–309.
9 M. Wagemaker, W. J. H. Borghols and F. M. Mulder, *J. Am. Chem. Soc.*, 2007, **129**, 4323–7.
10 W. J. H. Borghols, D. Lützenkirchen-Hecht, U. Haake, E. R. H. van Eck, F. M. Mulder and M. Wagemaker, *Phys. Chem. Chem. Phys.*, 2009, **11**, 5742–5748.
11 A. A. Belak, Y. Wang and A. Van der Ven, *Chem. Mater.*, 2012, **24**, 2894–2898.
12 A. Van der Ven, J. Bhattacharya and A. a Belak, *Acc. Chem. Res.*, 2013, **46**, 1216–25.
13 M. S. Whittingham, *J. Electrochem. Soc.*, 1977, 124, 1387.
14 F. Bonino, L. Busani, M. Lazzari, M. Manstretta, B. Rivolta and B. Scrosati, *J. Power Sources*, 1981, **6**, 261–270.
15 B. Zachau-Christiansen, K. West, T. Jacobsen and S. Atlung, *Solid State Ionics*, 1988, 28-30, 1176–1182.
16 K. Zhang, M. B. Katz, B. Li, S. J. Kim, X. Du, X. Hao, J. R. Jokisaari, S. Zhang, G. W. Graham, A. Van der Ven, B. M. Bartlett and X. Pan, *Adv. Mater.*, 2014, **26**, 7365–70.
17 D. P. Singh, A. George, R. V. Kumar, J. E. ten Elshof and M. Wagemaker, *J. Phys. Chem. C*, 2013, **117**, 19809–19815.
18 J. Qu, J. E. Cloud, Y. Yang, J. Ding and N. Yuan, *ACS Appl. Mater. Interfaces*, 2014, **6**, 22199–208.
19 Y.-G. Guo, Y.-S. Hu and J. Maier, *Chem. Commun. (Camb).*, 2006, 2783–2785.
20 P. Kubiak, J. Geserick, N. Hüsing and M. Wohlfahrt-Mehrens, *J. Power Sources*, 2008, **175**, 510–516.
21 J. Brumbarov and J. Kunze-Liebhäuser, *J. Power Sources*, 2014, **258**, 129–133.
22 J. Y. Shin, D. Samuelis and J. Maier, *Adv. Funct. Mater.*, 2011, **21**, 3464–3472.
23 a. R. Armstrong, G. Armstrong, J. Canales, R. García and P. G. Bruce, *Adv. Mater.*, 2005, **17**, 862–865.
24 J. S. Chen and X. W. Lou, *J. Power Sources*, 2010, **195**, 2905–2908.
25 J. Yan, H. Song, S. Yang and X. Chen, *Mater. Chem. Phys.*, 2009, **118**, 367–370.
26 S. K. Das and A. J. Bhattacharyya, *J. Phys. Chem. C*, 2009, **113**, 17367–17371.
27 B. Erjavec, R. Dominko, P. Umek, S. Sturm, a. Pintar and M. Gaberscek, *J. Power Sources*, 2009, **189**, 869–874.
28 J. Xu, C. Jia, B. Cao and W. F. Zhang, *Electrochim. Acta*, 2007, **52**, 8044–8047.
29 J. Li, Z. Tang and Z. Zhang, *Electrochem. Solid-State Lett.*, 2005, **8**, A316.
30 V. Zwilling, M. Aucouturier and E. Darque-Ceretti, *Electrochim. Acta*, 1999, **45**, 921–929.
31 D. J. LeClere, a. Velota, P. Skeldon, G. E. Thompson, S. Berger, J. Kunze, P. Schmuki, H. Habazaki and S. Nagata, *J. Electrochem. Soc.*, 2008, **155**, C487.
32 S. Leonardi, A. Li Bassi, V. Russo, F. Di Fonzo, O. Paschos, T. M. Murray, H. Efstathiadis and J. Kunze, *J. Phys. Chem. C*, 2012, **116**, 384–392.
33 J. M. Macak, H. Tsuchiya, a. Ghicov, K. Yasuda, R. Hahn, S. Bauer and P. Schmuki, *Curr. Opin. Solid State Mater. Sci.*, 2007, **11**, 3–18.
34 S. Ivanov, L. Cheng, H. Wulfmeier, D. Albrecht, H. Fritze and a. Bund, *Electrochim. Acta*, 2013, **104**, 228–235.
35 Z.-J. Zhang, Q.-Y. Zeng, S.-L. Chou, X.-J. Li, H.-J. Li, K. Ozawa, H.-K. Liu and J.-Z. Wang, *Electrochim. Acta*, 2014, **133**, 570–577.
36 H.-T. Fang, M. Liu, D.-W. Wang, T. Sun, D.-S. Guan, F. Li, J. Zhou, T.-K. Sham and H.-M. Cheng, *Nanotechnology*, 2009, **20**, 225701.
37 Q. L. Wu, J. Li, R. D. Deshpande, N. Subramanian, S. E. Rankin, F. Yang and Y. Cheng, *J. Phys. Chem. C*, 2012, **116**, 18669–18677.
38 K. Zhu, Q. Wang, J. H. Kim, A. a. Pesaran and A. J. Frank, *J. Phys. Chem. C*, 2012, **116**, 11895–11899.
39 D. Liu, Y. Zhang, P. Xiao, B. B. Garcia, Q. Zhang, X. Zhou, Y. H. Jeong and G. Cao, *Electrochim. Acta*, 2009, **54**, 6816–6820.
40 Z. Lu, C. T. Yip, L. Wang, H. Huang and L. Zhou, *Chempluschem*, 2012, **77**, 991–1000.
41 J. Shin, J. H. Joo, D. Samuelis and J. Maier, *Chem. Mater.*, 2012, **24**, 543–551.
42 R. Hahn, F. Schmidt-Stein, J. Sahnen, S. Thiemann, Y. Song, J. Kunze, V. P. Lehto and P. Schmuki, *Angew. Chemie - Int. Ed.*, 2009, **48**, 7236–7239.
43 N. Fairley, 2007.
44 J. M. Macak, H. Tsuchiya, L. Taveira, S. Aldabergerova and P. Schmuki, *Angew. Chemie - Int. Ed.*, 2005, **44**, 7463–7465.
45 J. Kunze, L. Müller, J. M. Macak, P. Greil, P. Schmuki and F. a. Müller, *Electrochim. Acta*, 2008, **53**, 6995–7003.
46 F. B. Growcock and R. J. Jasinski, *J. Electrochem. Soc.*, 1989, 136, 2310.
47 C. Valero Vidal and a. Igual Muñoz, *Electrochim. Acta*, 2010, **55**, 8445–8452.
48 P. Acevedo-Peña, M. Haro, M. E. Rincón, J. Bisquert and G. Garcia-Belmonte, *J. Power Sources*, 2014, **268**, 397–403.
49 C. Xu, Y. Zeng, X. Rui, J. Zhu, H. Tan, A. Guerrero, J. Toribio, J. Bisquert, G. Garcia-Belmonte and Q. Yan, *J. Phys. Chem. C*, 2013, **117**, 17462–17469.
50 L. Kavan, M. Grätzel, S. E. Gilbert, C. Klemenz and H. J. Scheel, *J. Am. Chem. Soc.*, 1996, **118**, 6716–6723.
51 R. Van De Krol, A. Goossens and J. Schoonman, *J. Phys. Chem. B*, 1999, **103**, 7151–7159.
52 O. T. Nanostructures, Q. Wang, Z. Wen and J. Li, 2006, **45**, 6944–6949.
53 D. Liu, P. Xiao, Y. Zhang, B. B. Garcia, Q. Zhang, Q. Guo, R. Champion and G. Cao, *J. Phys. Chem. C*, 2008, 11175–11180.

54 G. F. Ortiz, I. Hanzu, T. Djenizian, P. Lavela, J. L. Tirado and P. Knauth, *Chem. Mater.*, 2009, **21**, 63–67.

55 T. Pajkossy and D. M. Kolb, *Electrochim. Acta*, 2001, **46**, 3063–3071.

56 G. Sudant, E. Baudrin, D. Larcher and J.-M. Tarascon, *J. Mater. Chem.*, 2005, 1263–1269.

57 U. Lafont, D. Carta, G. Mountjoy, a. V. Chadwick and E. M. Kelder, *J. Phys. Chem. C*, 2010, **114**, 1372–1378.

58 S. K. Panda, S. Lee, W.-S. Yoon and H. Shin, *J. Power Sources*, 2014, **249**, 59–65.

59 M. S. Whittingham and B. M. Dines, *J. Electrochem. Soc.*, 1977, 124, 1387.

60 K. Shen, H. Chen, F. Klaver, F. M. Mulder and M. Wagemaker, *Chem. Mater.*, 2014, **26**, 1608–1615.

61 G. Sudant, E. Baudrin, D. Larcher and J.-M. Tarascon, *J. Mater. Chem.*, 2005, 1263–1269.

62 V. Likodimos, T. Stergiopoulos, P. Falaras, J. Kunze and P. Schmuki, *J. Phys. Chem. C*, 2008, **112**, 12687–12696.

Anatase TiO_{2-x}-C nanotubes demonstrate a superior Li storage capacity as high as 320(±68) mAh g^{-1} compared to 180(±38) mAh g^{-1} for TiO_{2-x}.

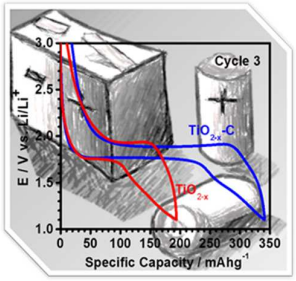

ToC figure 44 mm broad × 40 mm high

Authors: J. Brumbarov, J. P. Vivek, S. Leonardi, C. Valero-Vidal, E. Portenkirchner*, and J. Kunze-Liebhäuser

Title: Oxygen deficient, carbon coated self-organized TiO_2 nanotubes as anode material for Li-ion intercalation